Cite this article
Pham AT, Pham XD and Tan KH (2019)
Slab corner effect on torsional behaviour of perimeter beams under missing column scenario.
Magazine of Concrete Research **71(12)**: 611–623,
https://doi.org/10.1680/jmacr.18.00011

Research Article
Paper 1800011
Received 04/01/2018; Revised 08/02/2018;
Accepted 15/02/2018;
Published online 23/03/2018

Keywords: load transfer/structural analysis/structural design

Magazine of Concrete Research

ice Publishing

Slab corner effect on torsional behaviour of perimeter beams under missing column scenario

Anh Tuan Pham
Research Fellow, School of Civil and Environmental Engineering, Nanyang Technological University, Singapore

Xuan Dat Pham
Lecturer, Faculty of Building and Industrial Construction, National University of Civil Engineering, Ha Noi, Vietnam

Kang Hai Tan
Professor, School of Civil and Environmental Engineering, Nanyang Technological University, Singapore
(corresponding author: ckhtan@ntu.edu.sg)

Perimeter beams in reinforced-concrete buildings are subjected to considerable torsion from slab negative bending moments. In the event of progressive collapse caused by column removals, torsion effects on such beams become critical, owing to redistribution of loads. The aim of this study is to explore the effects of slab corners on the torsional behaviour of perimeter beams in reinforced concrete beam–slab buildings, particularly in the case of column loss. A series of torsional tests on peripheral beams was conducted, comparing cases with and without slabs. Thereafter, physics-based numerical models were developed, based on the test results, to investigate the effect of varying the slab's parameters, such as thickness and reinforcement ratio, on torsional capacity. The models showed that the presence of reinforced concrete slabs could increase the torsional strength of perimeter beams by as much as 97%. The enhancement came first from the slab corner, which acted as a set of compressive struts. This effect increased with increasing slab thickness. It was also observed that the slab corners tend to shift torsional failure (which occurred at the twisted beam near the support) to about one beam depth away. The contribution of negative bending moment from slab reinforcement along the edges could also enhance overall structural capacity.

Notation

A_0	total area surrounded by the shear flow path
A_g	area of the gross section of a solid beam
A_{oh}	area enclosed by the centre line of the outermost closed transverse torsional reinforcement
A_t	area from one closed stirrup leg
f'_c	concrete cylinder compressive strength
f_t	tensile strength of concrete
f_{yt}	stirrup yield strength
q	shear flow
s	stirrup spacing
T	torsional moment
T_{cr}	cracking torsional moment
T_n	torsional strength
t	wall thickness
U_g	outer perimeter of the gross section of a solid beam
V_{side}	vertical shear force
z	height between the top and the bottom chords of the strut-and-tie model
ε_{ij}	strain components
ε_{max}	maximum principal strain
θ	angle of strut
τ	shear stress

Introduction

In a conventionally designed reinforced-concrete (RC) building structure, negative bending moment in a slab may cause its supporting beam to twist. Interior beams may be subjected to insignificant torsional moment since the slab negative bending moment at one side of the beam is counterbalanced (to a large extent) by that at the other side. Perimeter beams along the edges of a floor plan, however, are subjected to compatibility torsion since slabs only exist at one side. While compatibility torsion may not be critical and can be neglected in the usual design case, it needs to be considered when resisting progressive collapse. Currently, modern codes of practice (ACI, 2011; CEN, 2004) allow beam torsional effect to be designed independently from slab action. Critical beam sections are often assumed to be near the faces of supporting columns and the maximum design torsional moments can be obtained from a linear elastic analysis. The required amount of stirrups and longitudinal reinforcement for the critical section is calculated based on codified formulations of torsional cracking and strength. In some conditions where moment redistribution is possible, design moments can be reduced provided that torsional cracking is allowed, together with some detailing requirements for adjoining members, such as slabs. In exterior corners of slabs supported by perimeter beams, additional reinforcement is required at both the top and the bottom slabs to control cracking and to resist bending moments resulting in the slab areas.

In a column removal scenario, however, the negative bending moments at slab discontinuous edges can be increased significantly, owing to load redistribution from the removed

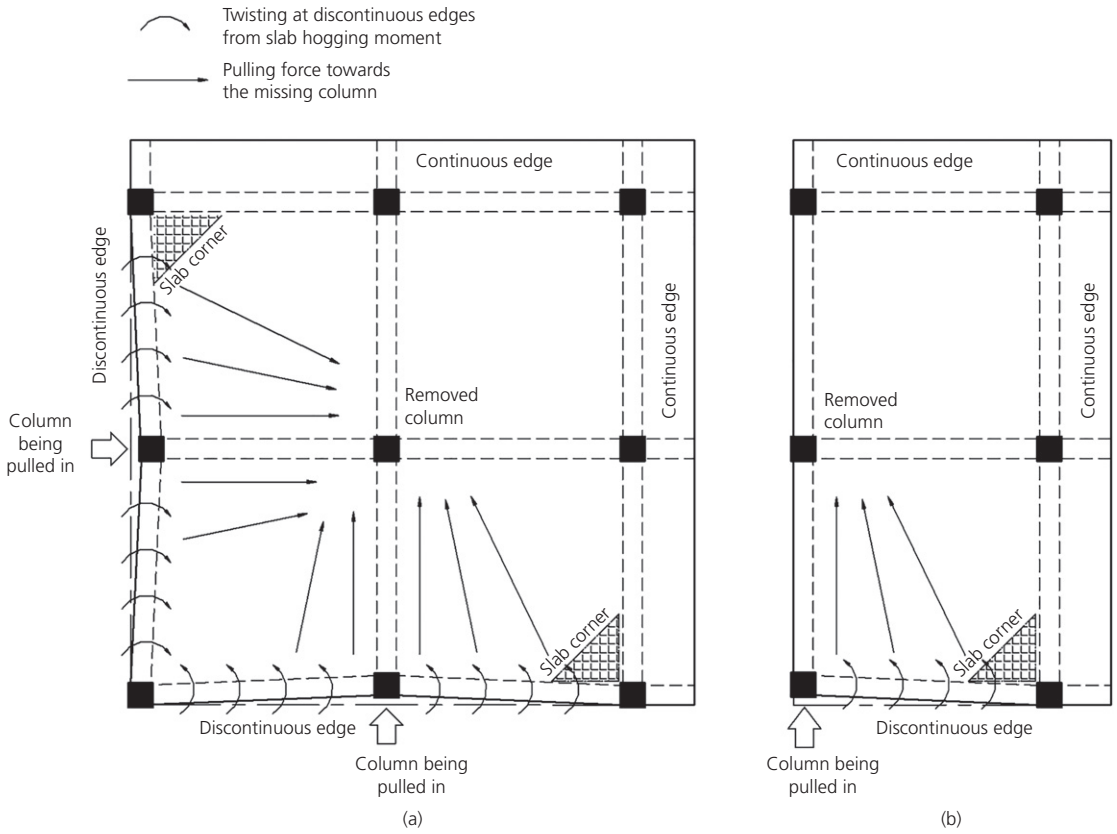

Figure 1. Twisting of peripheral beams under column removal scenarios: (a) internal column; (b) external column

column to adjacent intact columns. Previously, most studies on progressive collapse only concentrated on frame behaviour (FarhangVesali *et al.*, 2013; Qian and Li, 2012; Sadek *et al.*, 2011; Su *et al.*, 2009; Yi *et al.*, 2008; Yu and Tan, 2013), neglecting the effect from the slab system on top, and only a limited number of beam–slab tests were conducted (Lu *et al.*, 2017; Qian *et al.*, 2014). A recent study of RC beam–slab structures under different scenarios of column removal (Pham *et al.*, 2017a) showed that structural resistance under either internal or external column removal is even smaller than under the corner column case. It is due to torsional failure in peripheral beams, which in turn reduces the negative bending capacity of slabs at the edge. Figures 1(a) and 1(b) respectively show the effect of torsional moment on discontinuous edges of beam–slab systems under internal and external column removal scenarios.

Conversely, experimental studies on large-scale beam–slab substructures under missing column scenarios (Pham and Tan, 2013, 2015) show that although current torsional design procedure ignoring slab contribution is conservative, it does not adequately reflect the combined effect of beam–slab sections near supporting column faces. Figures 2(a) and 2(b) respectively show a beam–slab substructure loaded to failure using a loading-tree system to represent a uniformly distributed load, and the development of torsional cracks from its perimeter beams (Pham, 2013). As can be seen, the first torsional crack (at a load of 130 kN) appeared at a distance of at least twice the beam depth from the beam–column junction. Towards the end of the test, additional cracks developed farther away from that junction, and the test load was greater than previously thought. Hence, it is expected that in beam–slab structures the slab corners can greatly enhance the torsional behaviour of perimeter beams. For RC buildings with normal design under gravity loads, this effect can be conservatively ignored. Nonetheless, it becomes more important for progressive collapse mitigation when large deformations occur and the remaining structure has to seek alternate load paths to withstand collapse.

In modern RC buildings, perimeter beams are often required to be thin enough to align with non-load-bearing walls of less than 200 mm thick. In some cases where there are no walls, shallow beam depth is required to maximise the external view. In both instances, the provision of adequate torsional strength and stiffness of these perimeter beams becomes critical. In such situations, enhancement from slab corners can be considered in the design procedure. Most previous research studies on RC beams subjected to torsion (Collins and Lampert, 1973; Elfgren *et al.*, 1976; Ewida and McMullen, 1981;

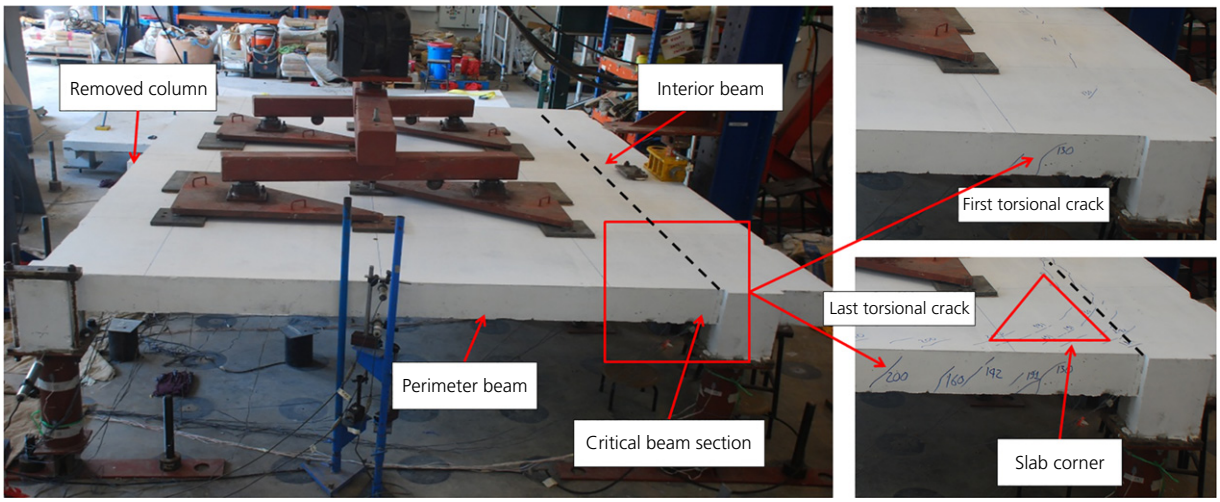

Figure 2. Torsional behaviour of perimeter beam subjected to uniform vertical load (Pham, 2013): (a) test setup; (b) torsional cracks of perimeter beams

Hsu, 1968; McMullen and Rangan, 1978; Mitchell and Collins, 1974; Rahal and Collins, 1995) were conducted on isolated beams without slabs. In these reported studies, critical sections for torsional failure were normally located at interfaces between the beam and its supports. However, in the presence of slabs, the location of torsional failure is shifted away from the beam end. To date, there is no experimental work, to our knowledge, on the interaction between perimeter beams and slab corners with regard to column-loss scenarios.

Testing programme

Test setup

A series of four RC specimens, named M1 to M4, was cast and tested, including two without slabs and two with slabs. A typical test setup for the no-slab specimens (M1 and M3) is presented in Figure 3, which shows Beam A, Beam B, and a test beam. Beam A was fully fixed to a strong laboratory floor by two vertical supports using concrete blocks SP-1 and SP-2 (200 mm depth) at its two ends plus a 30 mm dia. bolt at the midspan position tightened to the strong floor. Beam B was a cantilever beam subjected to a hydraulic load at its free end. The test beam (cast between Beam A and Beam B) was subjected to pure torsion. The end of the test beam at the intersection with Beam B was vertically supported by a steel hemisphere of 25 mm dia. (SP-3), allowing the section to be twisted freely. Vertical displacement at the loading point of Beam B was measured by a 50 mm displacement transducer, whereas the applied load from the hydraulic jack was monitored using a load cell. For the specimens with slabs (M2 and M4), a 60 mm thick RC slab was cast on top of the three beams. Such a test setup represented a substructure containing the slab corner from a beam–slab system that undergoes column removal (Figure 1).

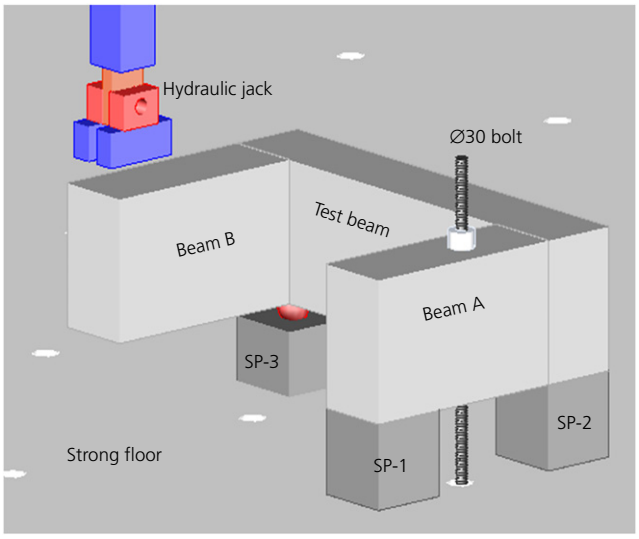

Figure 3. Typical test setup for specimens without slabs

Figure 4 shows the reinforcement details of the four specimens. The clear span of the test beam was 600 mm for M1 and M2 and 300 mm for M3 and M4. All beams were designed with the same cross-section (150 mm wide and 250 mm deep). The longitudinal reinforcement included four deformed bars with a diameter of 10 mm and a yield strength of 328 MPa; the stirrups were round bars of 6 mm diameter and 320 MPa yield strength, at a uniform spacing of 70 mm. The average cylinder compressive strength of concrete was 18 MPa. The torsional lever-arm, which was the distance from the loading point at Beam B to the centre of the test beam, was 350 mm in all the tests. The slabs in M2 and M4 were reinforced with a top layer of 6 mm round bars at 150 mm spacing in both directions. Table 1 shows the information for all four specimens.

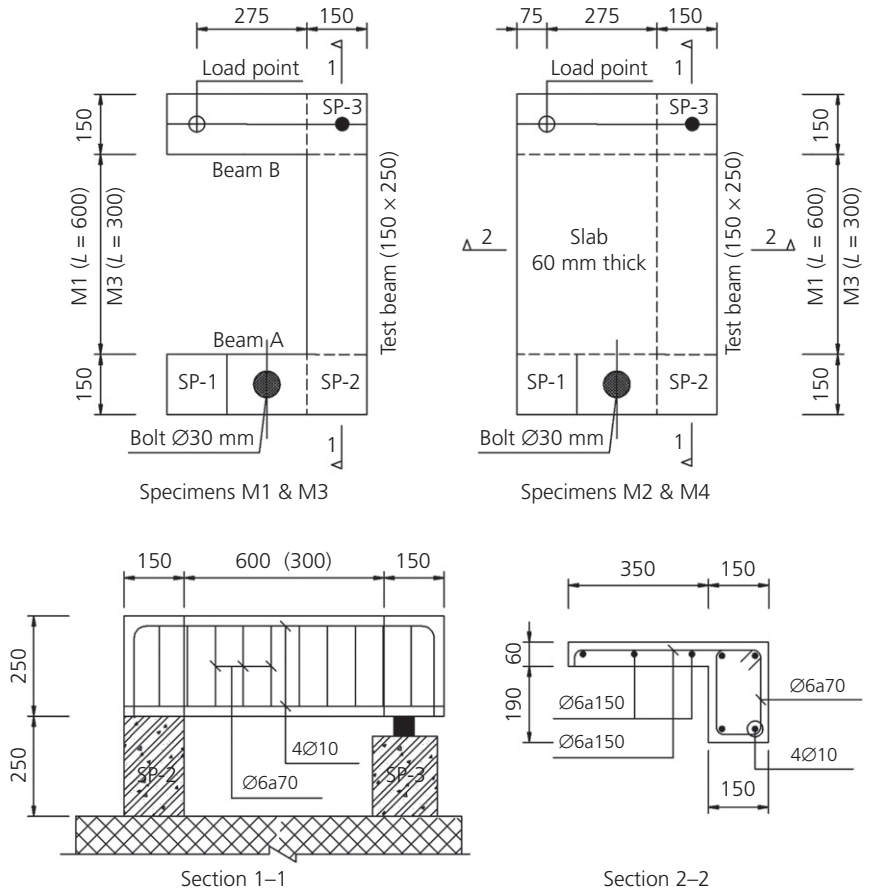

Figure 4. Specimen design (dimensions: mm)

Table 1. Test plan

Specimen ID	Test beam clear span: mm	Structure type
M1-B-600	600	Beam only
M2-S-600	600	Beam with slab
M3-B-300	300	Beam only
M4-S-300	300	Beam with slab

Test results

Figure 5(a) demonstrates the load-versus-displacement (at load point) relationship of specimens M1 (no slab) and M2 (with slab). In M1, as applied load increased, the first crack occurred at a load of 12 kN, at both the inner and the outer faces of the test beam, as shown in Figure 6(a). The displacement corresponding to this load was 2·0 mm. On increasing the load, inclined cracks continued to occur towards the loaded beam (Beam B). All the cracks had the same inclined angle, approximately 45°. The specimen attained its first peak load of 13·7 kN at a displacement of 2·6 mm, followed by a minor reduction in applied load as the displacement was increased. Thereafter, the applied load increased again and attained a maximum value of 21 kN at a displacement of 22·9 mm. Finally, the applied load slowly reduced until the test ended at a displacement of 38 mm. All the cracks on the outer, top and inner surfaces of the test beam were connected to each other, forming a spiral pattern along the beam longitudinal axis. The cracks on the inner and outer surfaces were perpendicular to each other. All torsional cracks on the outer surface were relatively uniform and inclined at an angle of about 45°.

For M2, with a 60 mm thick slab, the first crack was observed on the slab top surface, corresponding to an applied load of 22·5 kN and a displacement of 7·09 mm (Figure 5(a)). There was a slack in the load–displacement curve, probably due to the presence of some gaps in the setup. As the load increased, cracks started forming on the test beam. Both the slab and the test beam cracks had an inclined angle of 45° (Figure 6(b)). Thereafter, new cracks kept forming at the inner surface of the test beam (Figure 6(c)), as well as at the bottom surface of the slab. Similar to that of M1, the structural response of M2 saw a minor drop of capacity after the first peak of 22·9 kN at 6·8 mm deflection. As the displacement kept increasing, M2 gained a maximum capacity of 31·9 kN at a final deflection of 22·76 mm. Compared with the torsional cracks on the test beam of M1 (Figure 6(a)), those of M2 were shifted farther from the

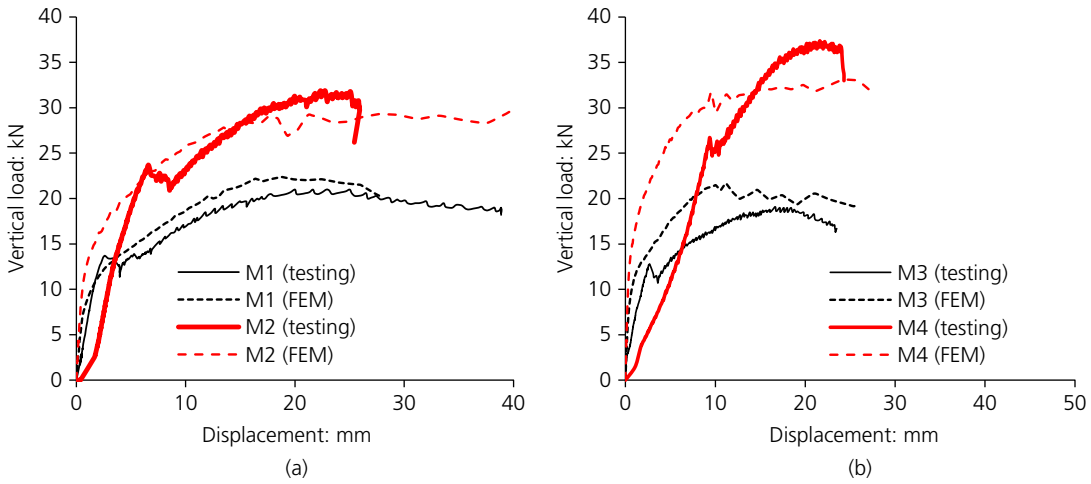

Figure 5. Load–displacement curves of all specimens: (a) M1 and M2; (b) M3 and M4

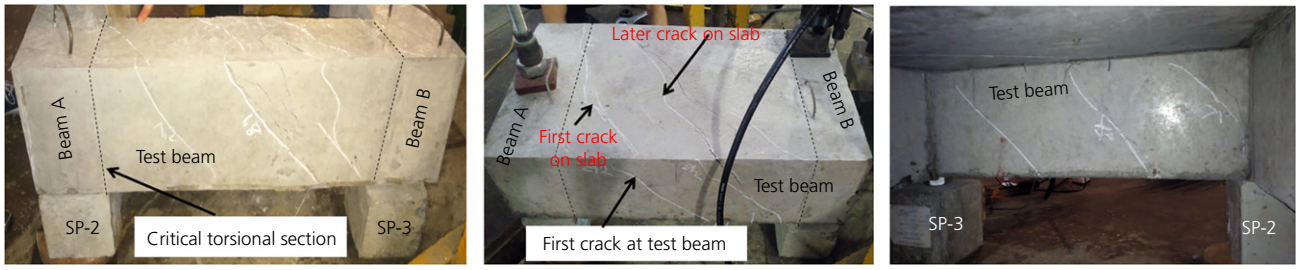

Figure 6. Crack patterns of specimens M1 (without slab) and M2 (with slab): (a) M1 (top and outer surfaces of test beam); (b) M2 (outer surface of test beam and slab top surface); (c) M2 (inner surface of test beam)

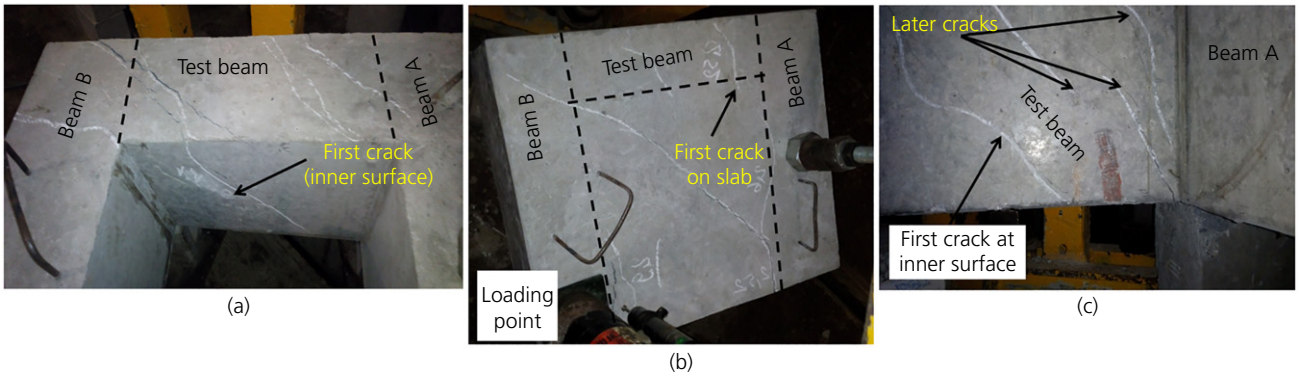

Figure 7. Crack patterns of specimens M3 (without slab) and M4 (with slab): (a) M3 (cracks at top and inner surfaces); (b) M4 (cracks at slab top surface); (c) M4 (cracks at test beam inner surface)

critical section (i.e. the interface with Beam A), as shown in Figure 6(b). A discussion of the finite-element predictions, shown in Figure 5(a), is presented in the section 'Numerical models for verification'.

For M3 without slab and with a clear span of 300 mm (Figures 5(b) and 7(a)), the first crack occurred at the outer surface of the test beam, corresponding to an applied load of 10·9 kN and a displacement of 2·06 mm. Thereafter, cracks started occurring at the inner and the top surfaces. However, along the outer surface, only one inclined crack was formed. The maximum capacity of the specimen was 19 kN, corresponding to a displacement of 18·1 mm. For M4 (Figures 5(b), 7(b) and 7(c)), cracks occurred first at the slab top surface, similar to

M2, then propagated to the outer surface of the test beam. The cracking load was 25·2 kN. Subsequently, cracks started occurring at the slab bottom and the test beam inner surfaces. The ultimate load-carrying capacity of this specimen was 37·4 kN.

In all the tests, the load–displacement curves shared a common trend: shortly after torsional cracks had appeared, the applied load reached the first peak, followed by a slight reduction of load and then a steady increase to the maximum load before failure, as seen in Figure 5. This phenomenon, which is not observed in other types of structural behaviour, such as flexure or shear, can be explained by the redistribution of shear stress due to torsional moment from the concrete cover to stirrups in the test beam. With increasing displacement just after the first peak load, the torsional cracks widened so that concrete cover carried no tension and became ineffective in resisting torsional moments. When the shear stress was fully transferred to the stirrups, applied load increased again and reached a maximum value.

Table 2 shows the test results corresponding to the first crack occurrence and the first peak of applied load, as well as when the maximum capacity was reached, for all four specimens. Comparing the behaviour of the tested structures with and without slabs, the enhancement in maximum capacity was obvious for those with RC slabs with the increase varying from 52% to 97%. Comparing between no-slab structures with different test beam clear spans, M3, with a span of 300 mm, had smaller maximum capacity (19 kN) compared with M1, with a span of 600 mm (21 kN). However, this difference was insignificant. Based on the applied load and torsion lever-arm (350 mm), the corresponding torsional moments in the test beam were calculated as shown in Table 2. In M1, the cracking moment corresponding to the first crack appearance was 4200 Nm. This value remained for a short range of torsional rotation and then increased to a maximum value of 7350 Nm. In M2, the cracking and ultimate torsional moments were 7875 Nm and 11 165 Nm, respectively, which were 88% and 52% higher than the corresponding values in M1. Similar observations were obtained when comparing M3 (without slab) and M4 (with slab). The cracking and ultimate torsional moments in M4 were 8820 Nm and 13 090 Nm, respectively, which were 132% and 97% larger than those of M2.

Comparisons between test results and predictions by ACI 318 and Eurocode 2

In two common codes of practice, ACI 318 (ACI, 2011) and Eurocode 2 (CEN, 2004), for RC structures, torsional resistance of a beam section is established following the same basis of a thin-walled closed section with the core concrete neglected, as illustrated in Figure 8(a). Shear flow q is calculated by the product of shear stress τ resulting from torsional

Table 2. Test results

	First crack			First peak of applied load		Maximum capacity		
	Load: kN	Torsional cracking moment T_{cr}: Nm	Displacement: mm	Load: kN	Displacement: mm	Load: kN	Torsional ultimate moment T_n: Nm	Displacement: mm
M1-B-600	12	4200	2·00	13·7	2·6	21	7350	22·9
M2-S-600	22·5	7875	7·09	22·9	6·8	31·9	11 165	22·76
M3-B-300	10·9	3815	2·06	12·8	2·69	19	6650	18·1
M4-S-300	25·2	8820	6·00	26·4	6·45	37·4	13 090	18·14

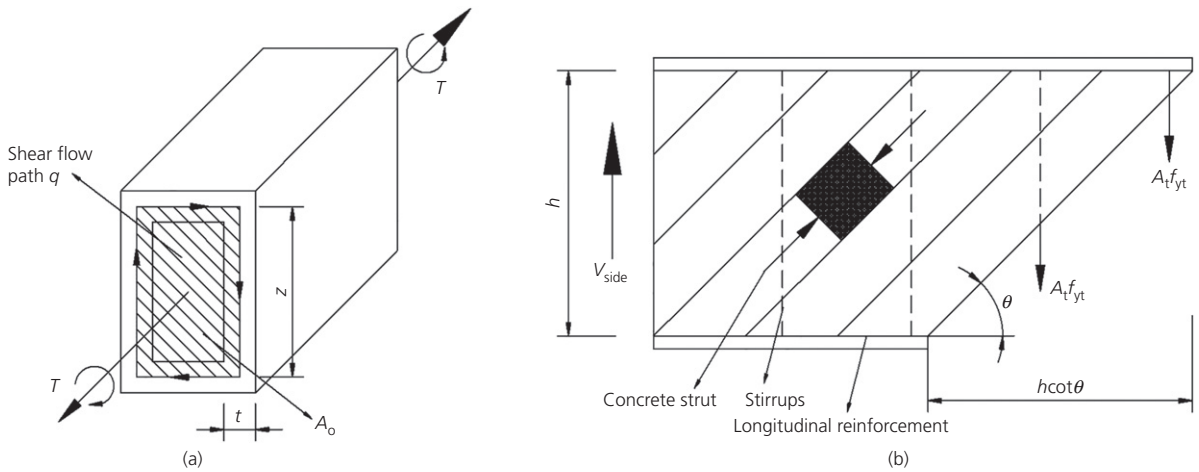

Figure 8. Thin-wall tube and strut-and-tie model for torsion calculation: (a) thin-wall tube analogy: (b) strut-and-tie model of a side wall

moment T, and wall thickness t ($q = \tau t$). Along the thin wall, q is constant and is given as

$$q = T/(2A_0) \quad (1)$$

where A_0 is the total area surrounded by the shear flow path.

In serviceability limit state design, the cracking torsional moment T_{cr} is calculated with the shear stress τ reaching the tensile strength of concrete f_t, as

$$T_{cr} = 2f_t tA_0 \quad (2)$$

Table 3 provides recommended values of the wall thickness t and the enclosed area A_0, in terms of the outer perimeter U_g and area A_g of the gross section of a solid beam, following ACI-318 and Eurocode 2. The calculations of t and A_0 are quite different between the two codes, and the product of tA_0 in Eurocode 2 is consistently higher than that in ACI, as can be seen in Table 3. For RC beams with normal size, the ratio of $(A_g/U_g)^3$ over tA_0 is approximately 10%. The values of cracking torsional moment T_{cr} according to the two codes are shown in Table 4. These predictions are based on the same value of f_t – that is, equal to $0{\cdot}33\sqrt{f'_c}$, where $f'_c = 18$ MPa is the concrete cylinder compressive strength.

In ultimate limit state design, torsional strength T_n is obtained from the strength calculation of a side wall subjected to shear force V_{side} due to T_n. A strut-and-tie model employed for strength calculations is illustrated in Figure 8(b) with three components: (*a*) concrete compression diagonal struts at angle θ, (*b*) tension ties of longitudinal reinforcement and (*c*) tension ties of closed stirrups. It is assumed that the concrete is fully cracked and does not resist any tension, while reinforcement has reached yield strength. The vertical shear force V_{side} acting on the side wall is given as

$$V_{side} = qz = \frac{T_n}{2A_0} z \quad (3)$$

Table 3. Recommended values of t and A_0 in ACI 318 and Eurocode 2

Code	t	A_0	tA_0
ACI 318	$0{\cdot}75A_g/U_g$	$2A_g/3$	$A_g^2/(2U_g)$
Eurocode 2	A_g/U_g	$A_g/2 + (A_g/U_g)^2$	$A_g^2/(2U_g) + (A_g/U_g)^3$

Table 4. Calculation of cracking torsional moment T_{cr} of the test beam

Code	A_g: mm^2	U_g: mm	tA_0: mm^3	f_t: MPa	T_{cr}: Nm
ACI 318	37 500	800	878 906	1·4	2461
Eurocode 2			981 903		2749

Table 5. Calculation of torsional strength T_n of the test beams according to ACI 318 (ACI, 2011) and Eurocode 2 (CEN, 2004)

Code	A_0: mm^2	A_t: mm^2	f_{yt}: MPa	s: mm	cotθ	T_n: Nm
ACI 318	25 415·2	28·23	320	70	1	6354·2
Eurocode 2	20 947·5					5237·1

where z is the height between the top and the bottom chords of the strut-and-tie model.

For a beam cross-section, the torsional strength T_n is predicted based on three criteria: compression failure of concrete struts, tension failure of longitudinal reinforcement and, most importantly, tension failure of stirrups. The strength calculation of a side wall based on tension failure of stirrups under vertical shear force V_{side}, as illustrated in Figure 8(b), can be computed as

$$V_{side} = \frac{T_n}{2A_0} z = \frac{A_t f_{yt}}{s} z \cot\theta \quad (4)$$

so that

$$T_n = \frac{2A_0 A_t f_{yt}}{s} \cot\theta \quad (5)$$

where A_t is the area from one closed stirrup leg, s is the stirrup spacing and f_{yt} is the stirrup yield strength.

Table 5 provides the predictions of torsional strength T_n according to ACI 318 (ACI, 2011) and Eurocode 2 (CEN, 2004). It is noteworthy that in ACI prediction, the gross area enclosed by the shear flow path is determined as $A_0 = 0{\cdot}85A_{oh}$ where A_{oh} is the area enclosed by the centreline of the outermost closed transverse torsional reinforcement.

Table 6 compares the test results and the values predicted by both ACI (ACI, 2011) and Eurocode (CEN, 2004). Generally, the two codes underestimated the cracking moment of the test beam, particularly for specimens with slab corners (M2 and M4). Conversely, relatively good agreement of ultimate torsional strength between the test results and the code predictions was obtained for specimens M1 and M3 (without slabs). In summary, the presence of the RC slab in M2 and M4 significantly enhanced the cracking and the ultimate torsional resistance of the test beam. Therefore, both codes' predictions are too conservative when they ignore the contribution of the slab.

Numerical models for verification

After conducting the four torsion tests, physics-based numerical simulations were employed to study the effect of different parameters on the contribution of the slab corner. Explicit finite-element modelling (FEM) program LS-Dyna (Hallquist, 2007) was employed to model the substructure

Table 6. Comparisons between test results and code predictions

	Cracking moment T_{cr}			Ultimate strength T_n		
Specimen	Test: Nm	Test/$T_{cr\ (ACI)}$	Test/$T_{cr\ (EC2)}$	Test: Nm	Test/$T_{cr\ (ACI)}$	Test/$T_{cr\ (EC2)}$
M1-B-600	4200	1·71	1·53	7350	1·16	1·4
M2-S-600	7875	3·2	2·86	11 165	1·76	2·13
M3-B-300	3815	1·55	1·39	6650	1·05	1·27
M4-S-300	8820	3·58	3·21	13 090	2·06	2·5

tests, owing to its numerical stability, as well as a wide variety of available constitutive models. Concrete was modelled with eight-node solid elements while rebars were simulated using two-node beam elements. Perfect bonding between reinforcement and concrete materials was assumed by applying the keyword 'Constrained_Lagrange_In_Solid'.

Material model

The continuous surface cap model (CSCM) MAT_159 in the LS-Dyna material library was employed to simulate the behaviour of the concrete material, owing to its stability, accuracy and user-friendliness (Bao *et al.*, 2014; Pham *et al.*, 2017a, 2017b). In this material model, the ultimate strength of concrete is characterised to be dependent on pressure as well as shear stress. When a uniaxial load is applied, deformation follows a linear elastic range, while concrete is considered isotropic. However, when the deformation is further increased, causing the stress to reach a peak value, there will be a reduction in stiffness and strength of concrete material. When the properties of the concrete material attain the yield surface, the concrete is assumed to start to fail. When damage occurs, the strength of concrete is reduced, leading the strength surface to collapse in the stress space. Besides the yield surface, the MAT_159 model employs two other surfaces to represent the maximum stress as well as the residual strength, named the limit and the residual surfaces. Irreversible damage will take place when the stress state reaches the limit surface, causing the collapse of the stress state towards the residual surface, which represents the total damage stage of the material. A cap is also employed on the yield surface to take into account an elastic limit within the stage of pure hydrostatic compression (Murray, 2007). In CSCM, two forms of damage are considered, ductile and brittle. Ductile damage is formed when the pressure is compressive. This type of damage depends on the total strain components (ε_{ij}). Conversely, brittle damage is formed when the pressure is tensile, depending on the maximum principal strain (ε_{max}).

The CSCM can be invoked through simple keyword input, which mostly depends on the compressive strength of concrete. Other related parameters can then be computed directly from the model. Three input data are required for CSCM: unconfined compressive strength, size of aggregate and the model units. The automatic generating function of CSCM is reliable for concrete with normal compressive strength (including stiffness, yield strength, hardening and damage).

Concerning steel reinforcement simulation, the Mat_Piecewise_Linear_Plasticity model (MAT_024) was employed. A convergence study was carried out, employing three mesh sizes: 25, 12·5, and 6·25 mm. As a result, the mesh size of concrete elements was chosen as 6·25 mm for the numerical simulations. The length of the rebar elements was also chosen as 6·5 mm. Figure 9 describes the FEM models of specimens M3 and M4 with a mesh size of 6·25 mm, whereas Figure 10 shows the modelling of reinforcement (using two-node beam elements) for specimen M2.

Validation results

The explicit analysis procedure in LS-Dyna was used to ensure stability and convergence. The loading point was forcibly moved downwards through a displacement-controlled regime until the reaction force was reduced significantly. Numerical predictions in terms of applied load versus displacement (at the loading point) were compared with the test results, shown in Figure 5. For the specimens with a test beam clear span of 600 mm (M1 and M2), the numerical models gave reasonably good agreement with the test data for both structural capacity and stiffness (Figure 5(a)). For M3 and M4, with a clear span of 300 mm for the test beam (Figure 5(b)), the FEM models overestimated the initial stiffness of specimen M4 (before cracks occurred). This may be due to imperfections in the setup of this specimen – for example, gaps in connections or slipping of supports during testing – which led to slack in stiffness at the beginning of the test. For the specimens with slabs, numerical predictions underestimated the maximum load by 7% and 10% for M2 and M4, respectively. Overall, LS-Dyna models slightly overestimated the displacements of the tests, showing that the concrete model used in the validation (CSCM) was less brittle than the actual material. Moreover, the numerical models could not capture the first peak when torsional cracks started occurring. However, they could still provide reasonably good predictions in terms of maximum structural capacity (when both longitudinal rebars and stirrups had been fully mobilised) compared with the test results, which is more critical in ultimate limit stage torsional design (Table 7).

Regarding failure mode, the FEM models provided similar damage patterns to the crack regions observed in actual tests. For the specimens without slabs, diagonal damage of concrete occurred on the top of the inner surfaces of the test beam,

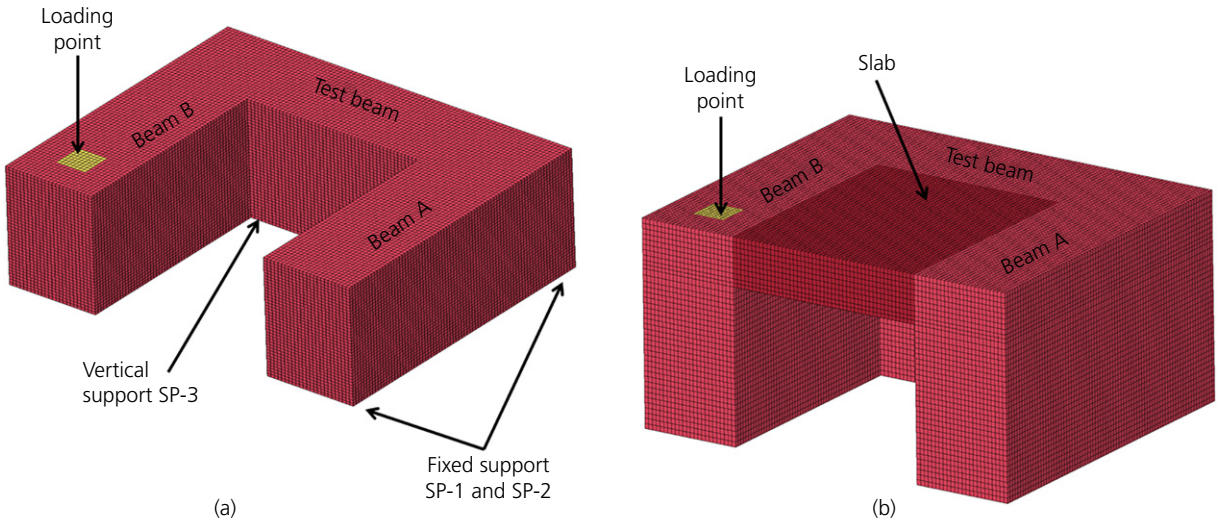

Figure 9. Finite-element models: (a) M3; (b) M4

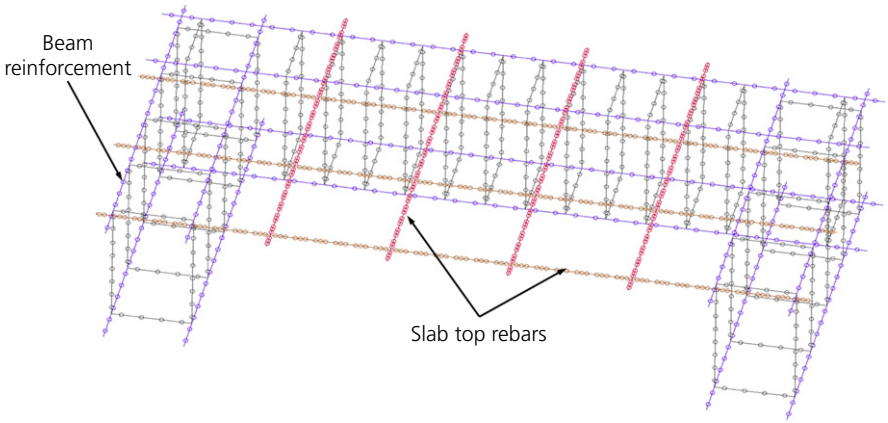

Figure 10. Reinforcement modelling (M2)

as shown in Figure 11. For the specimens with RC slabs (Figure 12), concrete damage was found developing along the slab edge with the fixed beam (Beam A), which also agreed with observations. Inclined damage also occurred at the inner surface of the twisted beam.

Parametric studies

After the verification studies, the FEM models were used to investigate different factors contributing to the enhancement of torsional capacity, especially those related to the presence of RC slabs.

Effect of slab thickness

Model M4 was rerun with different slab thickness values; the results are shown in Figure 13. As the slab thickness increased, the maximum load-carrying capacity increased accordingly. These results were reasonable, as a greater slab thickness leads to an increase in torsional capacity of the beam. The model with the 90 mm slab had almost 70% higher ultimate capacity than the one without a slab (i.e., the M3 model).

Table 7. Numerical validation

Specimen	Ultimate capacity: kN		
	Test	Finite-element modelling	Finite-element modelling/test
M1-B-600	21	22	1·05
M2-S-600	31·9	29·6	0·93
M3-B-300	19	21·12	1·11
M4-S-300	37·4	33·5	0·90

Effect of torsional beam length (no slab)

Besides the simulation results from models M1 and M3 (i.e., with test beam clear spans of 300 and 600 mm, respectively), different clear spans were also studied, including 450, 900 and

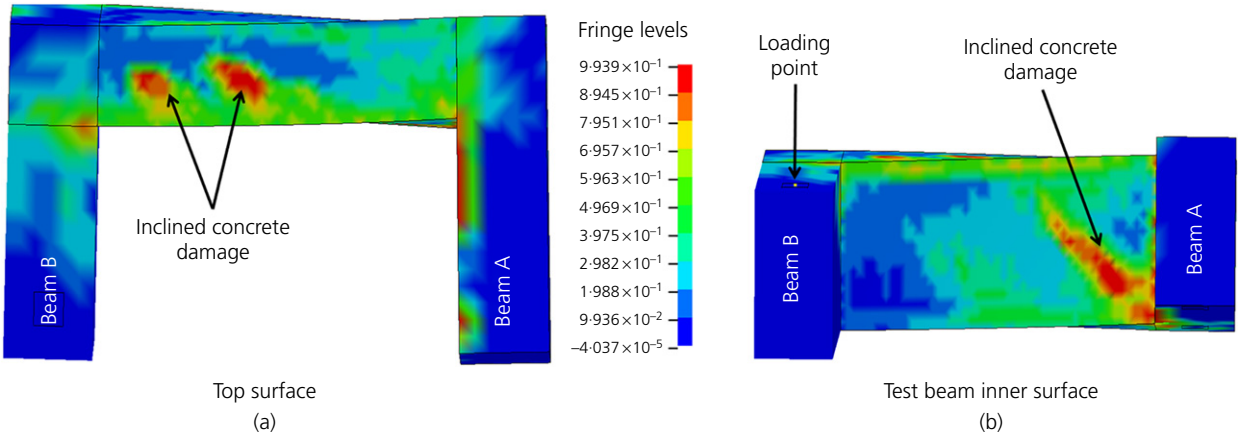

Figure 11. Failure modes of M1 model

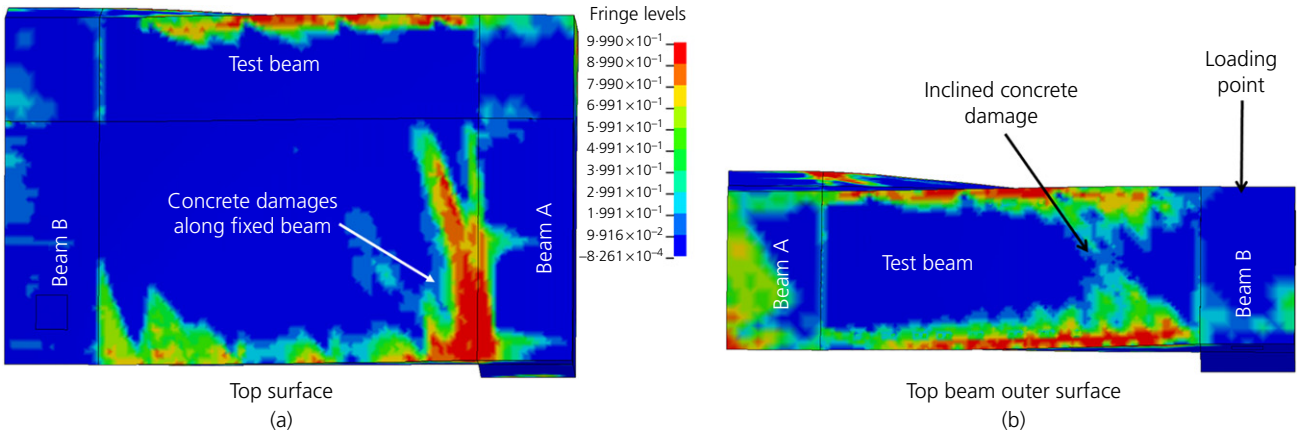

Figure 12. Failure modes of M2 model

1200 mm. The results (Figure 14) showed that beam length did not remarkably affect the torsional capacities of the specimens without slabs. Instead, models with longer spans had smaller stiffness values. As the span reached 900 mm and beyond, this influence became less significant. This finding of similar strength for different beam spans agreed well with code provisions for torsional resistance (ACI, 2011; CEN, 2004) which are based on cross-section dimensions and in which the beam span is not considered. However, in the presence of the RC slab, this assumption might not be correct.

Effect of slab reinforcement

To study the effect of slab reinforcement, the model of specimen M4 (with a test beam clear span of 300 mm) was used, varying the slab reinforcement diameter from 6 mm to 4 mm. Another model with the concrete slab but without any reinforcement was also employed, together with the results from the M3 model (no slab). Numerical results (Figure 15) show that slab reinforcement significantly influenced the

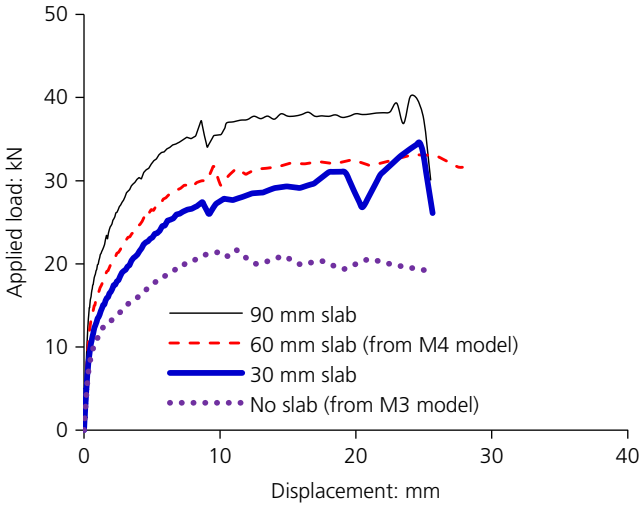

Figure 13. Effect of slab thickness

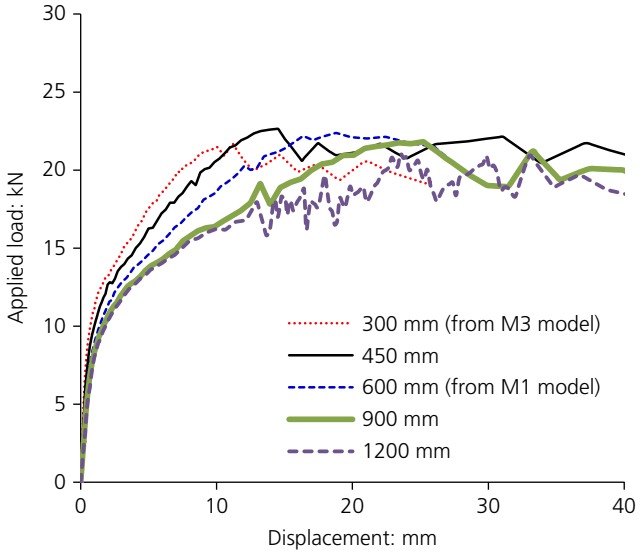

Figure 14. Effect of torsional beam length

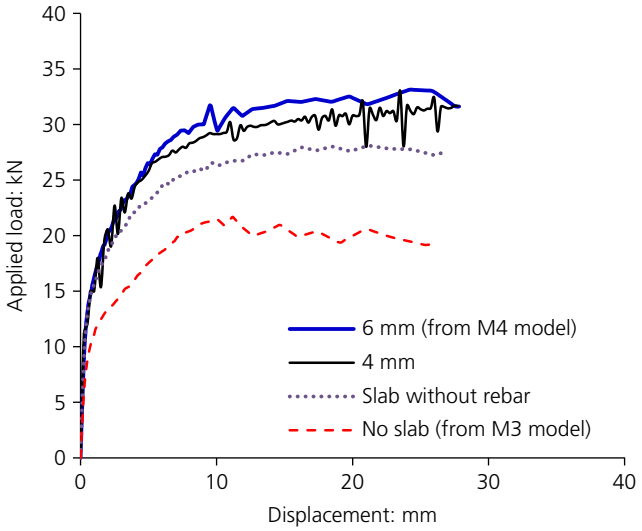

Figure 15. Effect of slab reinforcement diameter

structural capacity. While the model with slab but without slab reinforcement could increase the ultimate capacity by 40% compared with that without the slab (M3), the models with slab rebar diameters of 4 and 6 mm resulted in a further increase of 30 and 35%, respectively.

Effect of combined torsion–flexure loading

In buildings, perimeter beams are under the combined effects of flexure and torsion. Therefore, to incorporate the effect of flexure, all the four models of M1 to M4 were re-analysed without the support SP-3. As a result, the test beam was under both flexural and torsional moments created by the point load applied at the free end of Beam B. Results from these analyses were compared with those under pure torsion, as presented in Figure 16. Clearly, under combined torsion–flexure action, structural capacity was reduced significantly. For specimens M1, M2 and M3, the presence of flexural force reduced the structural capacity by 24, 26 and 13%, respectively. For M4, however, this reduction was only 6%. This was because M4 had a longer test beam clear span, which allowed more slab rebars to be mobilised along this edge, together with the effect of the slab corner.

Discussions on the effect of slab corner on beam torsional capacity

From actual test results (Figures 6 and 7), as well as material damages observed in the models (Figures 11 and 12), the general behaviour of torsional cracks on the test beam can be summarised as follows. For specimens without slab (M1 and M3), torsional cracks started developing at the interface with the support – that is, Beam A (Figure 17(a)). Conversely, for specimens with slabs (M2 and M4), torsional cracks on the test beam followed the first crack occurring on the slab. This created a triangular region on the slab corner bounded by Beam A and the test beam, acting as a compression truss and preventing the test beam from twisting (Figure 17(b)). As a result, the presence of the slab corner shifted the first torsional crack on the test beam farther away from the support location. As the slab thickness increased, the ultimate compressive strength of the truss also increased, thereby enhancing the overall structural resistance, as shown in Figure 13.

Besides the contribution of the slab corner as an analogous truss, slab reinforcement also helped to improve the ultimate capacity of the test beam, as shown in Figure 15. To shed light on the contribution of slab reinforcement, rebar tensile stresses extracted from the numerical results of model M2 are presented in Figure 18. These values were taken at a deformation of 12 mm when the slab top rebars started yielding. Along the slab edge at Beam A, the rebar tensile stress gradually increased when the rebar was placed farther from the slab corner. A similar phenomenon was also observed for rebars placed along the test beam edge. Therefore, it was concluded that within the slab corner area, slab reinforcement was less mobilised compared with adjacent steel bars along the two slab edges farther away from the corner. However, the contribution of negative bending moment at slab edges to the overall capacity of the specimen is also demonstrated, compared with those without slabs (M1 and M3). This contribution, together with the strut action from the slab corner, significantly enhanced the torsional capacity of the test beam.

The presence of flexural action, together with torsion, significantly reduced the structural capacity, as shown in Figure 16. Thus, it is necessary to conduct experimental studies to investigate the combined effect on beam torsional resistance. For example, when the torsional moment is noticeably smaller than the bending moment, flexure becomes the dominant

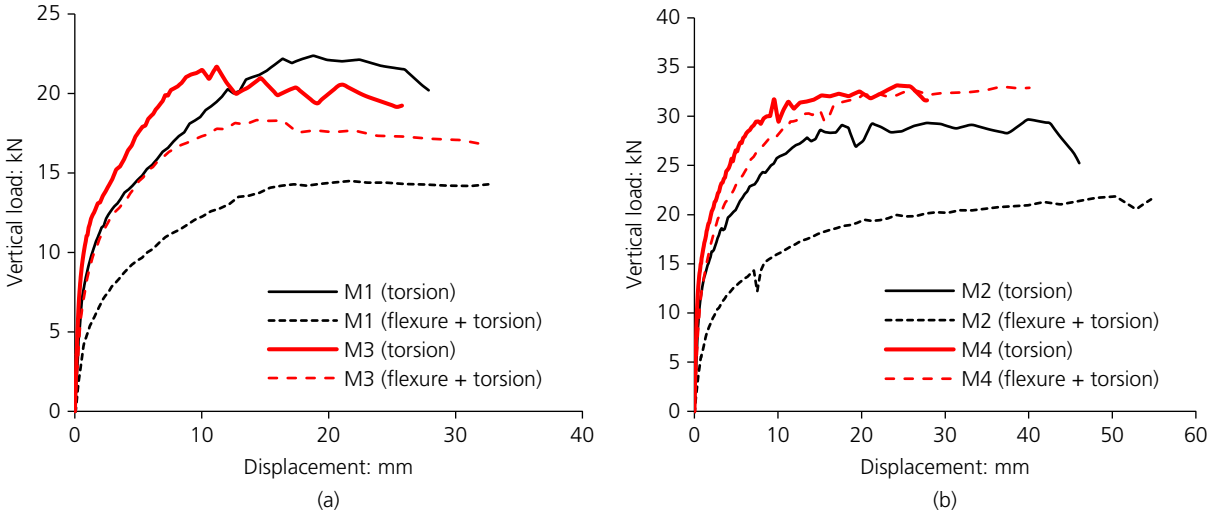

Figure 16. Effect of combined torsion–flexure: (a) specimens without slab; (b) specimens with slab

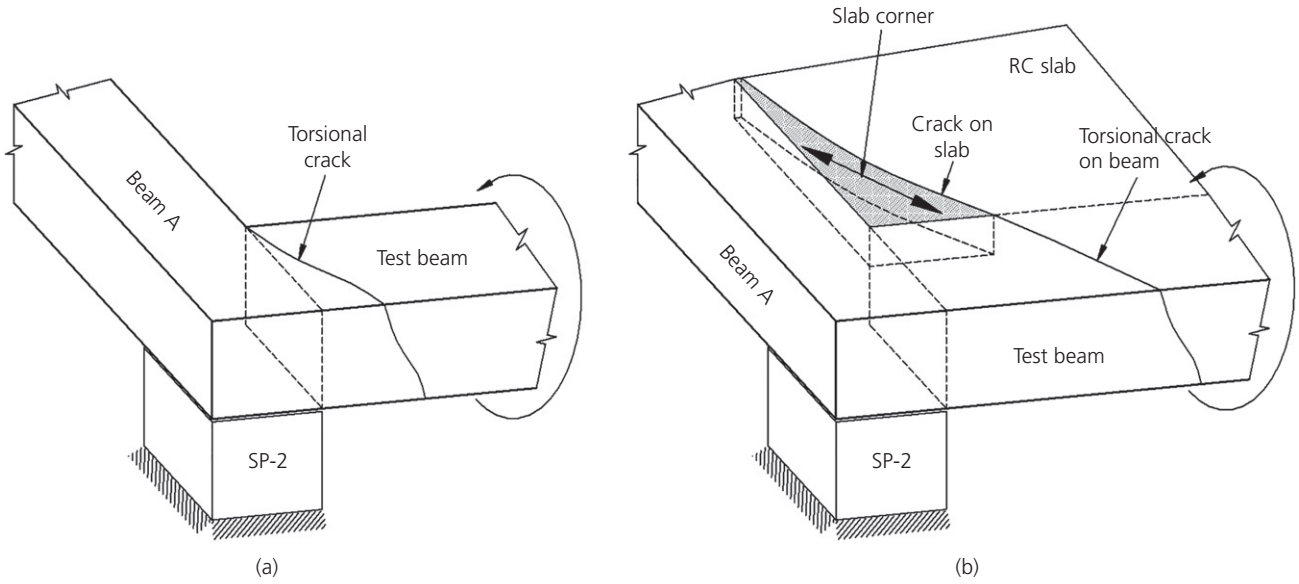

Figure 17. Torsional crack on test beam: (a) without slab; (b) with slab

action. In this case, the ultimate capacity of the test beam can be larger than the case under pure torsion.

Conclusions

In the design practice of RC buildings, torsion in perimeter beams is considered a secondary effect and is seldom taken into account in structural analysis. However, in some unexpected situations, such as missing column scenarios, the torsional strength of perimeter beams becomes more critical as it governs the collapse resistance of the remaining structures. In such cases, torsional strength assessment of the peripheral beams without any slab consideration may be too conservative and may not be suitable.

Experimental and numerical investigations conducted in this study showed that slab corners can significantly enhance the torsional behaviour of perimeter beams, especially under progressive collapse events. Cracking and ultimate capacities of the twisted beams with slab corners are as high as 232% and 197%, respectively, compared with specimens without any slabs. In the presence of slab corners, the critical beam section when torsional cracks started occurring was shifted farther from the support interface. The numerical investigation showed that both the slab thickness and the slab reinforcement had significant effects on the ultimate capacity of the test beam. While the slab corner itself could increase the capacity by more than 40%, the same amount of increase could be achieved due to slab

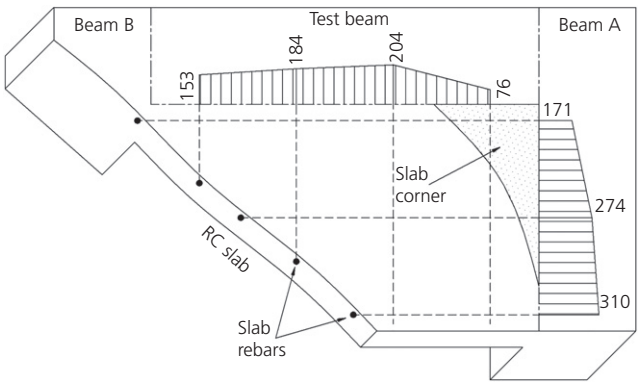

Figure 18. Distribution of tensile stress in slab reinforcement along the edges with Beam A and the test beam (dimensions: mm)

reinforcement. Therefore, it is recommended that RC slab corner areas on the top of perimeter beam–column connections should be properly detailed so that the enhancement of torsion strength of the beams can be considered when assessing progressive collapse resistance. Further experimental and analytical work is needed to quantify the contribution of the slab corner in enhancing the torsional capacity of perimeter beams.

Acknowledgements

The study presented in this paper was financially supported by the National Foundation for Science and Technology Development (NAFOSTED), Vietnam, through grant #107·01-2016·07. The financial support is greatly appreciated.

REFERENCES

ACI (American Concrete Institute) (2011) ACI 318-11: Building code requirements for structural concrete. American Concrete Institute, Farmington Hills, MI, USA.

Bao Y, Lew HS and Kunnath SK (2014) Modeling of reinforced concrete assemblies under column-removal scenario. *Journal of Structural Engineering* **140(1)**: 04013026.

CEN (European Committee for Standardization) (2004) 1992-1-1: 2004. Eurocode 2: Design of concrete structures – general rules and rules for buildings. European Committee for Standardization, Brussels, Belgium.

Collins MP and Lampert P (1973) *Redistribution of Moments at Cracking – The Key to Simpler Torsion Design?* American Concrete Institute, Farmington Hills, MI, USA.

Elfgren L, Karlsson I and Losberg A (1976) Torsion–bending–shear interaction for concrete beams: closure of discussion. *Journal of the Structural Division, Proceedings of the American Society of Civil Engineers, ASCE* **102(ST1)**: 289–291.

Ewida A and McMullen A (1981) Torsion–shear–flexure interaction in reinforced concrete members. *Magazine of Concrete Research* **33(115)**: 113–122.

FarhangVesali N, Valipour H, Samali B and Foster S (2013) Development of arching action in longitudinally-restrained reinforced concrete beams. *Construction and Building Materials* **47**: 7–19.

Hallquist JO (2007) *LS-DYNA Keyword User's Manual Version 971*. Livermore Software Technology Corporation, Livermore, CA, USA.

Hsu TTC (1968) *Torsion of Structural Concrete – Behavior of Reinforced Concrete Rectangular Members*. American Concrete Institute, Farmington Hills, MI, USA.

Lu X, Lin K, Li Y *et al.* (2017) Experimental investigation of RC beam–slab substructures against progressive collapse subject to an edge-column-removal scenario. *Engineering Structures* **149**: 91–103.

McMullen AE and Rangan BV (1978) Pure tension in rectangular sections – a re-examination. *ACI Journal Proceedings* **75(10)**: 511–519.

Mitchell D and Collins MP (1974) *Behaviour of Structural Concrete Beams in Pure Torsion*. University of Toronto, Department of Civil Engineering, Toronto, Canada.

Murray YD (2007) *Users Manual for LS-DYNA Concrete Material Model 159*. McLean, VA, USA.

Pham XD (2013) *Progressive Collapse of Reinforced Concrete Building Structures*. PhD thesis, Nanyang Technological University, Singapore.

Pham XD and Tan KH (2013) Experimental study of beam–slab substructures subjected to a penultimate-internal column loss. *Engineering Structures* **55**: 2–15.

Pham XD and Tan KH (2015) Experimental response of beam–slab substructures subject to penultimate-external column removal. *Journal of Structural Engineering* **141(7)**: 04014170.

Pham AT, Lim NS and Tan KH (2017a) Investigations of tensile membrane action in beam–slab systems under progressive collapse subject to different loading configurations and boundary conditions. *Engineering Structures* **150**: 520–536.

Pham AT, Tan KH and Yu J (2017b) Numerical investigations on static and dynamic responses of reinforced concrete sub-assemblages under progressive collapse. *Engineering Structures* **149**: 2–20.

Qian K and Li B (2012) Performance of three-dimensional reinforced concrete beam-column substructures under loss of a corner column scenario. *Journal of Structural Engineering* **139(4)**: 584–594.

Qian K, Li B and Ma JX (2014) Load-carrying mechanism to resist progressive collapse of RC buildings. *Journal of Structural Engineering* **141(2)**: 04014107.

Rahal K and Collins MP (1995) Analysis of sections subjected to combined shear and torsion – a theoretical model. *ACI Structural Journal* **92(4)**: 459–469.

Sadek F, Main JA, Lew HS and Bao Y (2011) Testing and analysis of steel and concrete beam-column assemblies under a column removal scenario. *Journal of Structural Engineering* **137(9)**: 881–892.

Su Y, Tian Y and Song X (2009) Progressive collapse resistance of axially-restrained frame beams. *ACI Structural Journal* **106(5)**: 600–607.

Yi WJ, He QF, Xiao Y and Kunnath SK (2008) Experimental study on progressive collapse-resistant behavior of reinforced concrete frame structures. *ACI Structural Journal* **105(4)**: 433–439.

Yu J and Tan KH (2013) Experimental and numerical investigation on progressive collapse resistance of reinforced concrete beam column sub-assemblages. *Engineering Structures* **55**: 90–106.

How can you contribute?

To discuss this paper, please submit up to 500 words to the editor at journals@ice.org.uk. Your contribution will be forwarded to the author(s) for a reply and, if considered appropriate by the editorial board, it will be published as a discussion in a future issue of the journal.